The Bacterial Quorum-Sensing Signal 2-Aminoacetophenone Rewires Immune Cell Bioenergetics through the PGC-1α/ERRα Axis to Mediate Tolerance to Infection

Arijit Chakraborty[1,2,3#], Arunava Bandyopadhaya[1,2,&#], Vijay K Singh[1,2], Filip Kovacic[1,3,4], Sujin Cha[1], William M. Oldham[5], A. Aria Tzika[1,2], and Laurence G Rahme[1,2,3*]

[1]Department of Surgery, Massachusetts General Hospital, and Harvard Medical School, Boston, Massachusetts, USA

[2]Shriners Hospitals for Children Boston, Boston, Massachusetts, USA

[3]Department of Microbiology, Harvard Medical School, Boston, Massachusetts, USA

[4]Institute of Molecular Enzyme Technology, Heinrich Heine University Düsseldorf, Forschungszentrum Jülich GmbH, Jülich, Germany

[5]Department of Medicine, Brigham and Women's Hospital and Harvard Medical School, Boston, Massachusetts, USA

[&] Present Address: Astellas Pharma Inc., USA

[#]These authors contributed equally

[*]**Corresponding author:** Laurence G. Rahme, Ph.D

e-mail: rahme@molbio.mgh.harvard.edu (LGR)

Address: 340 Their Research Building, 50 Blossom Street, Massachusetts General Hospital, Boston, MA 02114

Phone: 617-724-5003

Author Contributions:

Author contributions: L.G.R. conceptualization, A.B., A.C. and L.G.R., designed research; A.B., A.C. V.K.S., S.H.W., S. C., performed research; A.B., A.C. V.K.S., F.K., and L.G.R. analyzed data; W.M.O and A.A.T., provided resources, and F.K. and L.G.R. wrote the paper.

Competing Interest Statement:

L.G.R. has a financial interest in Spero Therapeutics, a company developing therapies to treat bacterial infections. L.G.R.'s financial interests are reviewed and managed by Massachusetts General Hospital and Partners Health Care in accordance with their conflict-of-interest policies. No funding was received from Spero Therapeutics, and it had no role in study design, data collection, analysis, interpretation, or the decision to submit the work for publication. The remaining authors declare no competing interests.

Classification:

Biological, health, and Medical Sciences/Microbiology

Keywords: Pseudomonas aeruginosa, quorum sensing, infection, macrophages, bacterial persistence, 2-aminoacetophenone (2-AA), MvfR, PqsR, immunometabolism, host tolerization, histone deacetylation, epigenetic reprogramming, metabolic reprogramming, oxidative phosphorylation, pyruvate, mitochondrial pyruvate carrier (MPC1), peroxisome proliferator-activated receptor gamma co-activator 1-alpha (PGC-1α), estrogen-related receptor (ERRα), acetyl-CoA, ATP, bioenergetics.

Abstract

How bacterial pathogens exploit host metabolism to promote immune tolerance and persist in infected hosts remains elusive. To achieve this, we show that *Pseudomonas aeruginosa (PA),* a recalcitrant pathogen, utilizes the quorum sensing (QS) signal 2-aminoacetophenone (2-AA). Here, we unveil how 2-AA-driven immune tolerization causes distinct metabolic perturbations in macrophages' mitochondrial respiration and bioenergetics. We present evidence indicating that these effects stem from a decrease in pyruvate transport into mitochondria. This reduction is attributed to decreased expression of the mitochondrial pyruvate carrier (MPC1), which is mediated by diminished expression and nuclear presence of its transcriptional regulator, estrogen-related nuclear receptor alpha (ERRα). Consequently, ERRα exhibits weakened binding to the MPC1 promoter. This outcome arises from the impaired interaction between ERRα and the peroxisome proliferator-activated receptor gamma coactivator 1-alpha (PGC-1α). Ultimately, this cascade results in diminished pyruvate influx into mitochondria and consequently reduced ATP production in tolerized macrophages. Exogenously added ATP in infected macrophages restores the transcript levels of *MPC1* and *ERR-α and* enhances cytokine production and intracellular bacterial clearance. Consistent with the *in vitro* findings, murine infection studies corroborate the 2-AA-mediated long-lasting decrease in ATP and acetyl-CoA and its association with *PA* persistence, further supporting this QS signaling molecule as the culprit of the host bioenergetic alterations and *PA* persistence. These findings unveil 2-AA as a modulator of cellular immunometabolism and reveal an unprecedent mechanism of host tolerance to infection involving the PGC-1α/ERRα axis in its influence on MPC1/OXPHOS-dependent energy production and *PA* clearance. These paradigmatic findings paving the way for developing treatments to bolster resilience to pathogen-induced damage. Given that QS is a common characteristic of prokaryotes, it is likely that 2-AA-like molecules with similar functions may be present in other pathogens.

Introduction

Host tolerance is a fundamental mechanism of innate immunity. Studies have shown that innate immune cells following infection or exposure to microbial products may enter a state of immune tolerance characterized by reduced responsiveness towards microbial re-exposure a few hours later [1-3]. Epigenetic and signaling-based mechanisms have been proposed to be involved in host immune tolerance [1-3]. In recent years, several reports have highlighted the complex interplay between metabolic reprogramming and immunity [4, 5]. It was suggested that specific metabolic programs are activated in monocytes and macrophages upon exposure to infection and microbial products [6, 7]. However, in host tolerance, the molecular mechanisms underlying immunometabolic reprogramming mediated by bacterial pathogens remain poorly understood.

Metabolic pathways are essential for generating energy for various cellular functions, including those performed by immune cells [8, 9]. Macrophages use metabolic pathways to generate energy and metabolites to adapt to changing environments and stimuli, thereby enabling them to cope with the needs of a fluctuating immune response [7, 10]. Thus, properly functioning metabolic pathways are vital for immune cells to counteract pathogens. For instance, the crucial energy-carrying molecule adenosine triphosphate (ATP) is required to phagocytose pathogen-derived molecules efficiently.

Pseudomonas aeruginosa (PA), a recalcitrant ESKAPE (*Enterococcus faecium, Staphylococcus aureus, Klebsiella pneumoniae, Acinetobacter baumannii, PA,* and *Enterobacter sp.*) pathogen that causes acute and persistent infections, secretes virulence-associated low molecular weight signaling molecules, several of which are regulated by quorum sensing (QS) [11-14] and able to modulate host immune responses [15-18]. QS is a cell density-dependent signaling system bacteria use to synchronize their activities [11-14]. MvfR (a.k.a. PqsR), a critical QS transcription factor of *PA,* regulates the synthesis of many small molecules, including signaling molecules such as 2-aminoacetophenone (2-AA) [11, 19-21]. *In vivo* studies have demonstrated that 2-AA enables *PA* to persist in infected murine

92 tissues by promoting innate immune tolerance through histone deacetylase 1 (HDAC1)-
93 mediated epigenetic reprogramming [17, 18]. 2-AA tolerization reprograms the host
94 inflammatory signaling cascade by maintaining chromatin in a "silent" state through increased
95 HDAC1 expression and activity and decreased histone acetyltransferase (HAT) activity [18].
96 These changes also impact the protein-protein interaction between HAT and cyclic AMP
97 response element-binding protein/HDAC1 and p50/p65 nuclear factor (NF)-κB subunits [18,
98 22]. The 2-AA-mediated tolerization permits *PA* to persist in infected tissues [17, 18]
99 underscoring the difference from lipopolysaccharide (LPS)-mediated tolerization, which
100 instead leads to bacterial clearance and involves different HDACs [23].

101 Mitochondria, the “powerhouse” of the cells, are crucial for the regulation,
102 differentiation, and survival of macrophages and other immune cells [8]. Our group's previous
103 *in vivo* and *in vitro* studies indicated that 2-AA affects metabolic functions in skeletal muscle,
104 which contains a high concentration of mitochondria [24-26]. Injection of 2-AA in murine
105 skeletal muscle dampens the expression of genes associated with OXPHOS and the master
106 regulator of mitochondrial biogenesis peroxisome proliferator-activated receptor-γ coactivator-
107 1 beta (PGC-1β) [24]. Another *PA* QS molecule, 3-oxo-C12-HSL, attenuates the expression of
108 PGC-1α [27]. PGC-1α and PGC-1β belong to the PPARγ family of inducible transcriptional
109 coactivators and are known regulators of mitochondrial metabolism [28]. The coactivator PGC-
110 1 proteins are involved in various cellular energy metabolic processes [29, 30], including but
111 not limited to mitochondrial metabolism [31]. Recent studies have also emphasized the role of
112 estrogen-related nuclear receptor α (ERRα) in coordinating metabolic capacity with energy
113 demand in health and disease [32]. PGC-1α activates ERRα transcriptional activity through
114 protein-protein interaction, which enhances the expression of ERRα [33, 34] and other
115 mitochondrial genes involved in lipid metabolism and OXPHOS [35]. PGC-1α/ERRα axis has
116 been extensively studied in cancer and established as a central regulatory node of energy
117 metabolism that induces the global expression of genes involved in mitochondrial biogenesis
118 and functions [36-38]. ERRα has been shown to occupy the promoter regions of many genes

119 participating in the TCA cycle and OXPHOS [39, 40], including the mitochondrial pyruvate
120 carrier (MPC1). In human renal carcinoma cells, PGC-1α/ERRα interaction results in efficient
121 activation of MPC1 expression and transport of pyruvate into mitochondrion for efficient
122 OXPHOS and energy production [41].

123 Given that our previous studies pointed to the 2-AA effect on mitochondrial functions
124 [24-26] and that mitochondria are crucial for the regulation, differentiation, and survival of
125 macrophages and other immune cells [8] we investigated how 2-AA may mediate cellular
126 metabolic reprogramming in tolerized immune cells by examining the link between the PGC-
127 1α/ERRα axis and 2-AA-mediated immune tolerance. Our findings uncovered the crucial action
128 of 2-AA on energy homeostasis and metabolism in tolerized immune cells through
129 perturbances of the ERRα/PGC-1α interaction, MPC1-mediated pyruvate transport and the
130 production of the key energy metabolism molecules, ATP and acetyl-CoA and their association
131 with the persistence of *PA* in mammalian tissues.

132

133

134 **Results**

135 **Tolerization by 2-AA impacts the generation of crucial energy metabolites in**
136 **macrophages**

137 Following infection or exposure to microbial products, innate immune cells may enter
138 a state of tolerance several hours later, as depicted by their diminished responsiveness or
139 unresponsiveness to microbial re-exposure [1-3, 42]. Given that 2-AA tolerized cells are non-
140 responsive to 2-AA re-exposure, we investigated the impact of 2-AA on energy homeostasis
141 and metabolism in non-tolerized and tolerized BMDM cells (Fig. 1). We quantified the levels of
142 ATP and acetyl-CoA, which is a fuel for ATP production, in a series of *in vitro* experiments in
143 which murine BMDM cells were exposed to 2-AA (1st 2-AA exposure) or re-exposed (2nd 2-AA
144 exposure) to respectively determine their activation, and tolerance as well as memory to this

145 QS molecule (Fig. 1A). Initially, following the 1st 2-AA exposure (black bars), a significant
146 increase in the concentrations of intracellular ATP (Fig. 1B) and acetyl-CoA (Fig. 1C) was
147 observed in BMDM cells exposed to 2-AA for 1 and 6 h compared to their corresponding naïve
148 control cells (grey bars). However, cells exposed to 2-AA for 48 h (black bar) appeared to have
149 entered a state of tolerance as ATP and acetyl-CoA levels were decreased compared to 2-AA
150 exposures for a shorter time (Figs. 1B and 1C). The tolerance of these cells as well as their
151 memory to 2-AA was determined by their responsiveness to a 2nd 2-AA exposure (Fig. 1A). To
152 achieve this, these cells were washed to remove 2-AA and allowed to rest for 24 or 106 h in
153 the absence of 2-AA before receiving the 2nd 2-AA exposure for 1 or 6 h (Fig. 1A). Figures 1B
154 and 1C (red bars) show the unresponsiveness of BMDM cells to 2-AA re-exposure as
155 evidenced by the similar levels of ATP and acetyl-CoA compared to cells exposed to 2-AA for
156 48 h (1st exposure black bars). The sustained unresponsiveness of the cells to re-exposure
157 indicates that the cells exhibited innate immunological memory, which could not be reverted
158 by 2-AA re-exposure. Similar responsiveness patterns of ATP and acetyl-CoA as with BMDM
159 cells were observed in murine macrophage RAW 264.7 cells (Figs. S1A and S1B) or human
160 monocyte THP-1 cells (Figs. S1C and S1D) following exposure or re-exposure to 2-AA. These
161 findings further support our observations with BMDM cells and confirm that either cell type can
162 be used to study responses to 2-AA. These results reinforce the notion that 2-AA impacts
163 crucial energy metabolites in macrophages.

164 Moreover, we sought to determine whether 2-AA-tolerized BMDM cells would respond
165 to heterologous stimulus. To test this, we re-exposed the cells to lipopolysaccharide (LPS), an
166 outer membrane bacterial component that strongly induces macrophages. LPS re-exposure of
167 the 2-AA tolerized BMDM cells did not significantly (p = 0.9) increase ATP levels (Fig. S2),
168 indicating that 2-AA cross-tolerized the cells to this heterologous bacterial immunostimulant.
169 On the other hand, as expected, we observed increased ATP levels following LPS stimulation
170 of the non-tolerized BMDM cells (Fig. S2). The broad spectrum of 2-AA cross-tolerization

171 strongly suggests an interplay of epigenetic mechanism rather than ligand-receptor mediated
172 signaling-based mechanism in bringing out the observed 2-AA-mediated tolerance.

173 **Tolerization by 2-AA leads to a quiescent state by reducing cell bioenergetics and**
174 **compromising OXPHOS.**

175 To further investigate the 2-AA's impact on the bioenergetics of macrophages, we
176 assessed by Seahorse assay the oxygen consumption rate (OCR) as an index of OXPHOS
177 in 2-AA exposed (for 1 and 24 h) and re-exposed (2nd exposure for 1 h) BMDM cells (Fig. 1D).
178 Values of basal (Fig. 1E) and maximal (Fig. 1F) mitochondrial respiration and spare
179 respiratory capacity (Fig. S3) interpreted from these measurements revealed that 1 h 2-AA
180 exposure of naïve cells significantly increased OCR compared to naïve control cells. At 24 h
181 post-2-AA exposure, cells had a significantly reduced basal OCR level than the control BMDM
182 cells, indicating decreased OXPHOS and an overall quiescent phenotype of tolerized
183 macrophages. Re-exposure of tolerized macrophages with 2-AA also did not augment
184 maximal and basal OCR (Figs. 1D-1F), indicating the unresponsiveness of tolerized BMDM
185 cells.

186 These OCR data are consistent with previous direct measurements of ATP (Fig. 1B)
187 and acetyl-CoA (Fig. 1C) and support the notion that 2-AA tolerization induces a quiescent
188 phenotype in these cells characterized by defective OXPHOS. These findings confirm that 2-
189 AA mediates energy homeostatic and metabolic alterations in the immune cells and that 2-AA
190 tolerization arrests these cells in a sustained 2-AA-unresponsive state.

191 **The pyruvate transport into mitochondria is decreased in tolerized macrophages.**

192 Since acetyl-CoA and ATP levels were reduced due to 2-AA tolerization, we
193 investigated whether the mitochondrial dysfunction observed is related to pyruvate
194 metabolism. Pyruvate links glycolysis with mitochondrial production of acetyl-CoA and ATP *via*
195 the tricarboxylic acid (TCA) cycle and OXPHOS [7]. RAW 264.7 cells initially exposed to 2-AA

196 for 1 or 3 h (black bars) exhibited significantly higher concentrations of cytosolic and
197 mitochondrial pyruvate compared to the corresponding naïve control cells (Fig. 2A). Pyruvate
198 significantly decreased over time in cytosolic and mitochondrial fractions as cells were entering
199 into the tolerized state (Fig. 2A). Tolerized cells remain unresponsive to 2-AA re-exposure (red
200 bars), exhibiting no significant change in the concentration of pyruvate in the cytosolic or
201 mitochondrial fraction (Fig. 2A). A similar result was observed in THP-1 cells (Figs. S1E and
202 S1F).

203 To gain a better understanding of the 2-AA-mediated reductions in mitochondrial
204 pyruvate, ATP production, and acetyl-CoA levels, we sought to determine the involvement of
205 the MPC1 [43] that is crucial in transporting pyruvate from the cytosol into the mitochondria
206 [44]. Western blot studies of whole cell lysates of RAW 246.7 cells exposed to 2-AA showed a
207 significant decrease over time in the abundance of MPC1 protein, and tolerized cells remain
208 unresponsive to 2-AA re-exposure (Fig. 2B). Together these findings suggest that 2-AA
209 tolerization dysregulates MPC1-mediated transport of the pyruvate into mitochondria.

210

211 **2-AA tolerization suppresses ERRα binding to the *MPC1* promoter and the interaction**
212 **between PGC-1α and ERRα**

213 Given that the PGC-1α/ERRα axis is the transcriptional regulatory node that activates
214 the expression of MPC1 [33] we determined the protein levels of ERRα. Western blot studies
215 of whole cell lysates showed a significant decrease over time in the abundance of ERRα
216 protein following 1st exposure of RAW 246.7 cells to 2-AA, while tolerized cells remain
217 unresponsive to 2-AA re-exposure (Fig. 3A). By assessing the cytosolic and nuclear
218 abundance of ERRα in tolerized cells we found that both fractions had lower levels of ERRα
219 protein than their corresponding control cells (Fig. 3B).

220 Furthermore, because an ERRα binding putative DNA motif (TNAAGGTCA) has been
221 identified upstream of the *MPC1* promoter in humans [43], and we found the same motif to be

222 present 1.5 kB upstream of the transcription start site of mouse *MPC1* promoter, we analyzed
223 if tolerization led to reduced ERRα binding to the *MPC1* promoter motif TNAAGGTCA.
224 Chromatin immunoprecipitation (ChIP) assay followed by qPCR analysis revealed that in
225 tolerized cells, ERRα binds approximately 4-fold less efficiently to the putative binding site on
226 the *MPC1* than in corresponding control cells (Fig. 3C).

227 Since the transcriptional activity of ERRα is regulated through a protein-protein
228 interaction with the transcriptional coactivator PGC-1α [33] we assessed whether the formation
229 of the PGC-1α/ERRα complex is affected in 2-AA tolerized cells. Using paraformaldehyde fixed
230 nuclear lysates of RAW 264.7 tolerized and naïve cells, we performed a co-
231 immunoprecipitation (co-IP) of PGC-1α and reverse co-IP with ERRα followed by
232 immunoblotting (Fig. 3D). As shown in Figure 3D less ERRα was detected when PGC-1α was
233 pulled down in presence of 2-AA than in naïve control cells. Moreover, reverse co-IP with ERRα
234 protein showed lower levels of PGC-1α in the presence of 2-AA than in naïve control cells (Fig.
235 3D). Control IgG showed no detectable levels of ERRα following nuclear fraction pull down.
236 These results indicate that in the tolerized macrophages, PGC-1α/ERRα interaction is impaired
237 (Fig. 3D).

238 Moreover, since PGC-1α enhances the transcriptional activity of ERRα through their
239 interaction, and ERRα transcription is regulated *via* an autoregulatory loop [34], we examined
240 the effect of tolerization on the transcription of *ERRα* and its target gene *MPC1*. Using RAW
241 264.7 cells infected with the wild type *PA* strain PA14 or isogenic Δ*mvfR* mutant, which does
242 not produce 2-AA [21] we observed lower RNA transcript levels of *MPC1* (Fig. 4A) and *ERRα*
243 (Fig. 4B) in PA14 compared to Δ*mvfR*. The addition of 2-AA to Δ*mvfR* decreased the levels of
244 both gene transcripts to t levels similar to the PA14 infection condition, supporting the role of
245 2-AA in effect. To test if the observed effects are due to MPC1-dependent reduction of
246 mitochondrial ATP generation, we supplemented the macrophages with ATP. The findings
247 indicate that the addition of ATP in PA14 infected cells elevated the transcript levels of both
248 *ERRα* and *MPC1*, but not in the Δ*mvfR* infected macrophages (Fig. 4A and 4B). These results

249 indicate that reduced MPC1 function is due to 2-AA tolerization on the transcriptional activation
250 of *MPC1* through the PGC-1α/ERRα axis.
251
252 **2-AA tolerization impairs macrophage-mediated intracellular bacterial clearance**
253 **through decrease in MPC1-mediated pyruvate import, ATP, and TNF-α levels.**

254 2-AA-mediates persistence of *PA in vivo,* dampens proinflammatory responses and
255 increases the intracellular burden of this pathogen in macrophages *via* epigenetic
256 modifications [17, 18, 26]. Here we used RAW 264.7 cells that were infected with the PA14 or
257 the 2-AA deficient Δ*mvfR* mutant to assess the clearance of *PA* by macrophages.
258 Macrophages infected with PA14 showed increased bacterial burden than the cells infected
259 with Δ*mvfR,* and 2-AA addition to Δ*mvfR* led to increased bacterial burden (Fig. 4C).
260 Furthermore, we used UK5099 and ATP to interrogate whether MPC1 mediated mitochondrial
261 pyruvate import and bioenergetics are linked to the clearance of *PA* intracellular burden. The
262 addition of the UK5099 inhibitor strongly enhanced the bacterial intracellular burden in Δ*mvfR*
263 infected macrophages compared to the non-inhibited cells (Fig. 4C). UK5099 had no effect on
264 the PA14 burden in macrophages. Conversely, exogenously added ATP to macrophages
265 infected with PA14 strongly reduced the *PA* intracellular burden (Fig. 4C).
266 Given that 2-AA tolerization decreases the expression of pro-inflammatory cytokine
267 TNF-α by hypo-acetylating the core histone 3 lysine 18 acetylation (H3K18ac) mark at TNF-α
268 promoter [18], we investigated the link between bioenergetics and TNF-α expression in
269 infected macrophages. UK5099, or ATP was added exogenously to infected macrophages with
270 PA14 or Δ*mvfR* (Fig. 4D). As shown in Figure 4D, PA14 infected cells showed lower TNF-α
271 transcript levels compared to the Δ*mvfR* infected cells. Supplementation of 2-AA to Δ*mvfR*
272 infected cells led to a decrease in the TNF-α transcript levels. Moreover, the addition of the
273 MPC1 inhibitor, UK5099 in Δ*mvfR* infected counteracted the increase in TNF-α transcript
274 levels, while had no effect in PA14 infected macrophages (Fig. 4D). Conversely, exogeneous

275 addition of ATP to PA14 infected cells enhanced the transcription of TNF-α compared to the
276 untreated PA14 infected cells, while no changes in TNF-α expression levels were observed in
277 Δ*mvfR* infected macrophages in presence of absence of ATP (Fig. 4D).These findings strongly
278 suggest that 2-AA tolerization severely alters macrophages' ability to facilitate the clearance of
279 *PA* intracellular burden, *via* the reduction in MPC1-mediated pyruvate import into mitochondria,
280 ATP levels and TNF-α transcription.
281
282 ***In vivo* studies corroborate the 2-AA-mediated decrease *in vitro* of the central metabolic**
283 **fuel acetyl-CoA and the energy-carrying molecule ATP and their association with *PA***
284 **persistence.**

285 To determine whether the decrease in the key metabolites mediated by 2-AA is also
286 observed *in vivo* during infection, we quantified the levels of ATP and acetyl-CoA in murine
287 spleen tissues at 1, 5, and 10 days (Fig. 5). This organ was selected for our immunometabolic
288 studies due to its role in regulating not only local but also systemic (whole-body) immune
289 responses, facilitated by various immune cells including macrophages [45]. Mice were infected
290 with *PA* strain PA14, or isogenic mutant Δ*mvfR,* which does not produce 2-AA [21]. It is
291 important to note that it is not possible to generate or utilize a bacterial mutant that is defective
292 in 2-AA only because 2-AA is formed by spontaneous decarboxylation rather than by an
293 enzyme-catalyzed reaction [46-48]. Therefore, animals that were either infected with Δ*mvfR*
294 and received 2-AA (Δ*mvfR*+2-AA) at the time of infection or uninfected mice injected with a
295 single dose of 2-AA served as direct controls (Fig. 5). Naïve and sham mice groups served as
296 additional basal controls (Fig. 5).

297 Infection with PA14 or uninfected mice injected with 2-AA led to a significant decrease
298 in both ATP (Fig. 5A) and acetyl-CoA (Fig. 5B) concentrations in spleen tissues compared to
299 Δ*mvfR* infected mice that sustained higher ATP and acetyl-CoA levels similar to naïve and
300 sham control groups across the time points tested. However, in mice infected with Δ*mvfR* and

301 2-AA injected *(Δmvf*R+2-AA) at the time of infection, ATP and acetyl-CoA concentrations in the
302 spleen decreased to levels comparable to those of PA14-infected animals, strongly indicating
303 the biological function of 2-AA in decreasing these key metabolites. These *in vivo* findings
304 further support the adverse action of 2-AA on host energy homeostasis and metabolism
305 observed *in vitro* studies.

306 The metabolic alterations observed are associated with the host tolerance to *PA*
307 persistence (Fig. 5C). Using *Pseudomonas* isolation agar plates, we evaluated the bacterial
308 load at the infection site over the course of 10 days, obtaining samples at 1, 5, and 10 days.
309 At one day post-infection, mice infected with PA14, Δ*mvfR,* or Δ*mvfR*+2-AA exhibited no
310 difference in bacterial burden (Fig. 5C), verifying the ability of all strains to establish infection.
311 At 5- and 10-days post-infection, mice infected with PA14 or Δ*mvfR*+2-AA sustained the
312 bacterial burden at a significantly higher bacterial burden over time compared to those infected
313 with Δ*mvfR* (Fig. 5C). These results are consistent with our previous findings [17, 18] and
314 provide compelling evidence that the metabolic alterations identified may favor *PA* persistence
315 in infected tissues.

316

317 **Discussion**

318 The *PA* signaling molecule 2-AA that is abundantly produced and secreted in human tissues
319 [21, 22] is the first QS molecule that epigenetically reprograms immune functions, promotes
320 immune tolerance, and sustains *PA's* presence in host tissues [17, 18, 22, 26]. The present
321 study provides insights into the mechanistic actions of 2-AA on cellular metabolism that
322 contribute to host immune tolerance to *PA* persistence. We uncover that this signaling
323 molecule causes distinct metabolic alterations in macrophages' mitochondrial respiration and
324 energy production promoted via the PGC-1α/ERRα axis and MPC1-dependent OXPHOS that
325 links the TCA cycle to the production of ATP and energy homeostasis (Fig. 6). Our results show

326 that 2-AA tolerization decreases ATP the crucial energy metabolite and the histone acetylation
327 metabolite acetyl-CoA and *in vivo*, implicating the importance of the key energy-producing
328 mitochondrial process in immune tolerance. Although macrophages respond to the first
329 exposure to 2-AA by enhancing ATP and acetyl-CoA production, long-term exposure to 2-AA
330 leads to a tolerized state characterized by sustained reduced ATP and acetyl-CoA
331 concentrations, a quiescent bioenergetic state with reduced mitochondrial pyruvate uptake and
332 unresponsiveness to a 2nd exposure.

333 Our results reveal that the decrease of ATP and acetyl-CoA in tolerized macrophages
334 results from the 2-AA-mediated perturbation of the physical interaction between ERRα and
335 PGC-1α. The PGC-1α/ERRα axis has not previously been implicated in tolerization but has
336 been extensively studied in cancer, underscoring the novelty of our findings. Studies in cancer
337 cells have shown that the physical interaction of human ERRα with PGC-1α strongly enhances
338 the binding of ERRα to DNA to induce the activation of the targeted genes [33] including *MPC1,*
339 responsible for the import of cytosolic pyruvate into mitochondria and PDH, that catalyzes the
340 conversion of pyruvate to acetyl-CoA in mitochondria. Inhibition of ERRα has been shown in
341 cancer cell metabolism studies to interfere with pyruvate entry in mitochondria by inhibiting the
342 expression of MPC1 [49]. Indeed, we find that the transcription of *ERRα* and *MPC1* genes
343 and pyruvate uptake into mitochondria is reduced in tolerized macrophages. Given that
344 pyruvate is a primary carbon source in the TCA cycle that fuels OXPHOS and the production
345 of ATP into mitochondria, it explains the reduced ATP and acetyl-CoA levels observed in
346 tolerized macrophages. Future studies will focus on unveiling the pathways by which
347 macrophages respond to the bioenergetic changes identified and decipher their effect on the
348 pyruvate cycle in host tolerance to infection [50-52].

349 We show that the unprecedented action of a QS bacterial small signaling molecule on
350 the interaction between ERRα and PGC-1α in the nucleus is hampered. Although it remains to
351 be elucidated whether 2-AA interferes directly or indirectly with the PGC-1α/ERRα axis, our
352 data bring up the possibility that the reduced production of acetyl-CoA may be responsible,

353 since cholesterol is a known coactivator/ligand of ERRα [53], is generated from acetyl-CoA
354 [53]. This possibility may also explain the reduced expression of *ERRα* and its lower
355 abundance since cholesterol is also required for its activation and autoregulation. However, it
356 is also possible that 2-AA may antagonize the interaction between ERRα and PGC-1α by
357 binding to ERRα. Small molecules as antagonist of ERRα have been reported previously [54].
358 The weaker binding of ERRα to the *MPC1* promoter site, and consequently reduced MPC1
359 expression explains the reduced pyruvate presence in mitochondria and that of ATP and
360 mitochondrial quiescence.

361 The observed cellular metabolic perturbances also align with our previous studies in
362 skeletal muscle, which pointed to mitochondrial dysfunction triggered by 2-AA [24, 25].
363 Interestingly, the *PA* QS LasR-regulated homoserine lactone molecule, 3-oxo-C12-HSL, was
364 reported to attenuate the expression of PGC-1α and decrease the mitochondrial respiratory
365 capacity in lung epithelial cells [27]. Moreover, another *PA* QS molecule PQS also regulated
366 by LasR was recently shown to induce organelle stress, including mitochondria, by disrupting
367 the mitochondrial membrane potential in human macrophages [55]. As opposed to 2-AA, which
368 dampens the pro-inflammatory response, PQS increases proinflammatory cytokines [55],
369 consistent with the fact that PQS is an acute infection type molecule unrelated to
370 chronic/persistent infections.

371 Previously, we reported that 2-AA tolerization induces HDAC1 expression and activity,
372 reducing H3K18ac at the TNF-α promoter [18]. The findings with TNF-α transcription using
373 UK5099 and ATP in 2-AA treated macrophages are in support of the bioenergetics
374 disturbances observed in macrophages and their link to epigenetic modifications we have
375 shown to be promoted by 2-AA [18]. Macrophages exposed to 2-AA in the presence of
376 exogenous ATP showed improved intracellular bacterial clearance and enhanced TNF-α
377 levels, supporting the epigenetic interconnection of macrophages and cellular ATP
378 responsiveness levels against infection. The exogenous addition of UK5099 that reverted the

379 efficiency of the *mvfR* infected macrophages to clear the *PA* intracellular burden and the
380 counteraction to the 2-AA effect by ATP addition that increases the clearance of *PA* intracellular
381 burden support the importance of this energy-carrying molecule in *PA* persistence.

382 The results with the MPC1 inhibitor, UK5099, suggest that the availability of pyruvate
383 could underlie the mechanism of 2-AA-regulated HDAC/HAT-dependent control of transcription
384 of pro-inflammatory mediators and bacterial clearance [56]. These results align with our
385 previous findings, showing that establishing bacterial intracellular burden in macrophages is
386 HDAC1 dependent [56]. It remains to be elucidated if HDAC/HAT-mediated histone
387 modification directly regulates expression of OXPHOS genes in 2-AA tolerized macrophages
388 as it was shown that histone deacetylation downregulates OXPHOS in persistent *M.*
389 *tuberculosis* infection [57, 58]. Given the complexity of 2-AA-mediated long-term effects, future
390 omics studies combined with immune profiling may aid in deciphering the possible network of
391 co-factors across different subpopulations of immune cells and the immunometabolic
392 reprogramming related to 2-AA.

393 We have shown that although 2-AA tolerization leads to a remarkable increase in the
394 survival rate of infected mice, it permits an HDAC1-dependent sustained presence of *PA* in
395 mice tissues and intracellularly in macrophages [17, 18, 22, 26]. Here, we use 2-AA-producing
396 and isogenic non-producing *PA* strains to confirm the 2-AA-mediated decrease in the central
397 metabolite acetyl-CoA and the energy-carrying molecule ATP during infection. These murine
398 infection studies provide strong evidence of the 2-AA biological relevance in reducing these
399 metabolites *in vivo*. Taking together our previous and current *in vivo* findings provide
400 compelling evidence that the metabolic alterations identified favor *PA* persistence in infected
401 tissues.

402 That 2-AA permits *PA* to persist in infected tissues despite rescuing the survival of
403 infected mice underscores its difference from that of LPS tolerization, which results in bacterial
404 clearance [23] *via* the mechanism that relies on a set of different HDAC enzymes. LPS

405 tolerization predominantly involves changes in H3K27 acetylation [59], while 2-AA tolerization
406 involves H3K18 modifications [22]. The 2-AA-mediated effects reported here are also distinct
407 from the epigenetic-metabolic reprogramming mediated by LPS [60], which promotes
408 endotoxin tolerance in immune cells by upregulating glycolysis and suppressing OXPHOS [61].
409 Although 2-AA and LPS implicate different components and lead to different outcomes both
410 involve epigenetic mechanisms and immune memory.

411

412 Metabolic reprogramming upon infection may be pathogen-specific, with each
413 pathogen impacting specific metabolic pathways that better fit its respective metabolic needs
414 [7]. This was shown for infections of various tissues with *Chlamydia pneumonia*, *Legionella*
415 *pneumophila*, *Mycobacterium tuberculosis*, and *Salmonella* [62-65] and, by our group, for *PA*
416 infections [17, 18, 24]. It would be interesting, however, to test whether 2-AA affects the killing
417 efficacy of macrophages against other pathogens, as emerging evidence shows that
418 synergistic or antagonistic interactions between clinically relevant microorganisms and host
419 have important implications for polymicrobial infectious diseases [66].

420 While in this study, we focused on the role of ERRα mainly in pyruvate metabolism,
421 future studies are needed to reveal other ERRα/PGC-1α axis-dependent metabolic and
422 immune pathways are modulated by 2-AA. In this view, the cholesterol synthesis pathway that
423 relies on acetyl-CoA precursor, as cholesterol is a known coactivator/ligand of ERRα [53] and
424 fatty acid catabolism, generating acetyl-CoA, and PGC-1α regulates fatty acid oxidation [67].

425 This study unveils the unprecedented actions of a QS bacterial molecule in
426 orchestrating cellular metabolic reprogramming in addition to the epigenetic reprogramming
427 reported previously also shown to promote a long-lasting presence of *PA* in the host [17, 18,
428 26]. That 2-AA cross-tolerized macrophages to LPS corroborates our previous findings on the
429 implication of epigenetic mechanism [18] rather than ligand-receptor mediated signaling-based
430 mechanism, and raises the possibility that this QS molecule may confer non-specific cross

431 protection. An aspect we plan to investigate in the future. The reported immunometabolic
432 reprogramming contributes to a better understanding of the molecular and cellular
433 mechanisms, biomarkers, and functional significance that may be involved in immune
434 tolerance to persistent infection, providing for designing and developing innovative
435 therapeutics and interventions. These approaches can focus on promoting host resilience
436 against bacterial burden and safeguarding patients from recalcitrant persistent infections.

437

438 **Materials & Methods**

439 **Ethics statement**

440 The animal protocol was approved by the Institutional Animal-Care and Use Committee
441 (IACUC) of Massachusetts General Hospital (protocol no. 2006N000093). No randomization
442 or exclusion of data points was applied.

443 **Conditions used for the exposures of the cells to 2-AA**

444 Mouse BMDM cells were isolated from femur of CD1 6 weeks old male and female mice and
445 used to estimate the levels of various metabolites (Fig. 2A) following exposure and re-exposure
446 to 2-AA (Fig. 1A). The 1st exposure of naïve BMDMs (10^6/mL in 6-well plates) was achieved
447 with 400 μM 2-AA for 1, 6, or 48 h. Cells exposed for 48 h were used for the 2nd 2-AA exposure.
448 These cells were washed to remove residual 2-AA, left in the medium in the absence of 2-AA
449 for either 24 or 106 h, and re-exposed to 2-AA (200 μM) for 1 or 6 h, respectively. For RAW
450 264.7 (10^6/mL in 6-well plates) and THP-1 cells (10^6/mL in 6-well plates) the 2-AA concentration
451 and conditions used were as with BMDM cells. The hours of the 1st round and 2nd round of
452 exposure to 2-AA are indicated in Figure S1.

453 For the LPS stimulation studies, cells were stimulated with 400 μM 2-AA or 100 ng/mL LPS for
454 6 h, and 800 μM of 2-AA for 48 h. Cells receiving 1st exposure for 48 h were washed and re-
455 exposed to 400 μM of 2-AA or 100 ng/mL LPS for 6 h.

456 **ATP and acetyl-CoA quantifications**

457 The levels of ATP, acetyl-CoA, and were assessed in BMDM and RAW264.7 macrophage cells
458 following exposure to 2-AA at the times indicated and by utilizing the ATP Assay kit
459 (cholorimetric/fluorometric) (#ab83355, Abcam) and the PicoProbe AcCoA assay kit (ab87546,
460 Abcam), respectively, according to the manufacturer's instruction. Quantifications of ATP and
461 acetyl-CoA were performed in triplicates.

462 ***ATP***: For ATP determination, macrophages were lysed and subsequently centrifuged at 14,000
463 rpm for 10 min at 4 °C. The supernatants were transferred to a fresh Eppendorf tube.
464 Standards and cell supernatants of 50 µL were added to a 96-well plate suitable for fluorescent
465 analysis (black sides, clear bottom). A reaction mixture containing an ATP converter, probe,
466 buffer, and developer mix was then added to all wells (50 µL) and incubated away from light at
467 room temperature for 30 min. ATP quantification was conducted fluorometrically at 535/587 nm
468 using a plate reader and the following settings: λex = 535 nm; λem = 587 nm. Fluorescence
469 was measured using a microplate reader (Tecan Group Ltd, Männedorf, Switzerland)

470 *Acetyl-CoA*: Acetyl-CoA content was assessed by first deproteinizing total cell fractions of
471 macrophages using the perchloric acid and then centrifuging at 14,000 rpm for 10 min at 4 °C.
472 50 µL of cells' supernatant sample CoASH were quenched to correct the background
473 generated by free CoASH. Following the homogenization procedure described above, the
474 samples were diluted with the reaction mix, and fluorescence was quantified using a plate
475 reader and the settings as above with ATP.

476 **Seahorse Assays**

477 Seahorse analysis was performed according to previously published protocols [68]. Briefly,
478 freshly prepared BMDM cells were reseeded in complete RPMI-1640 cells using Seahorse
479 plates (Agilent cat. no. 103729100) at a density of 5×10^4 cells per well. Cells were exposed
480 to 400 µM 2-AA for 1 h or 24 hours (1st exposure). Cells receiving 1st exposure for 24 h were

481 washed and re-exposed to 200 μM of 2-AA for 1 h. Naïve cells were used as control. Prior to
482 initiating Seahorse measurements cells were washed and Seahorse XF DMEM supplemented
483 with 2 mM glutamine (Gibco cat. No. 25030-081) was added to each well. Cells were allowed
484 to stabilize in a 37°C incubator without CO_2 for 1 h. The Seahorse cartridge was hydrated and
485 calibrated as per the manufacturer's instructions. The Mitochondrial stress test kit (Agilent cat.
486 no. 10395-100) was used (oligomycin at 1 μM, FCCP (1.5 μM), rotenone (0.5 μM), and
487 antimycin A at (0.5 μM)) with slight modifications according to the published protocol [68] that
488 included injection of 25 mM glucose, and sodium pyruvate (1 μM). All samples N= 4 were run
489 in a Seahorse XFe96 Analyzer, and data were analyzed using Wave and plotted using
490 GraphPad Prism software.

491 **Isolation of cytosolic and mitochondrial fraction and pyruvate quantification**

492 Pyruvate is produced in the cytosol and is transported into the mitochondria. RAW 264.7 cells
493 were plated at 1×10^6 to incubate overnight at 37°C in a CO_2 incubator. Cells were exposed to
494 2-AA for 1, 3, 24 or 48 h or re-exposed for 1 h as described above. Mitochondria and cytosolic
495 fractions of each group were isolated utilizing the Mitochondria Isolation Kit for cultured cells
496 (#ab110170, Abcam) following the manufacturer's protocol. Briefly, cells were collected with a
497 cell lifter and pelleted by centrifugation at 1,000 g, frozen, and then thawed to weaken the cell
498 membranes. The cells were resuspended in Reagent A and transferred into a pre-cooled
499 Dounce Homogenizer. The homogenates were centrifuged at 1,000 *g* for 10 min at 4°C and
500 saved as supernatant #1 for the cytosolic fractions. The pellet was resuspended in Reagent B,
501 followed by repeat rupturing and centrifugation. The pellet was collected and resuspended in
502 500 μL of Reagent C supplemented with Protease Inhibitor cocktails (P8340, Sigma Aldrich).
503 Following separation, a Bradford assay was conducted to determine the protein concentration
504 in each fraction. Pyruvate levels were determined in cellular fractions and mitochondrial
505 fractions by using the Pyruvate Assay Kit (#ab65342, Abcam) according to the manufacturer's
506 instructions. Briefly, after deproteinization using perchloric acid, the samples were neutralized

507 in ice-cold 2 M KOH. 10 µL samples were incubated with reaction mix and kept on the plate at
508 RT for 30 min in the dark. The absorbance was measured in a microplate reader (Tecan Group
509 Ltd, Männedorf, Switzerland) at 570 nm and results are shown from three independent
510 experiments.

511 **Bacterial strains and growth conditions**

512 The *PA* strain known as Rif^R human clinical isolate UCBPP-PA14 (also known as PA14) was
513 used [69]. The bacteria were grown at 37 °C in lysogeny broth (LB) under shaking and aeration
514 or on LB agar plates containing appropriate antibiotics. PA14 and isogenic mutant Δ*mvfR* [19]
515 cultures were grown in LB from a single colony to an optical density of 600 nm (OD_{600}) of 1.5,
516 diluted 1:50,000,000 in fresh LB media, and grown overnight to an OD_{600} of 3.0.

517 **Gentamicin protection assay**

518 RAW264.7 macrophage cells were plated on 6 well cell culture-treated plates overnight in
519 pyruvate free DMEM. After 3 h of incubation with 10 µM UK5099, 20 µM ATP or 400 µM 2-AA,
520 cells were infected with PA14 and isogenic mutant Δ*mvfR* at 5 MOI for 30 min at 37 °C in 5%
521 CO_2. Unbound bacteria were removed by washing once with cold DMEM medium. Afterwards,
522 the cells were incubated with 100 µg/ml of gentamicin for 30 min to eliminate residual
523 extracellular bacteria. The cells were washed with DMEM and transferred to free medium
524 without gentamicin and kept for 3 h at 37°C in 5% CO_2. The infected cells were scraped after
525 3 h, centrifuged at 500 × g, and lysed in distilled water. The lysed cells were immediately diluted
526 in PBS and plated on LB agar plates to assess bacterial presence. Bacterial colony-forming
527 units (CFUs) were counted after incubating the plates overnight at 37°C.Untreated cells
528 infected with PA14 were set as 100 % and the reduction of Bacterial load was expressed as
529 %CFU.

530 **Pharmacological inhibitors and ATP supplementations**

531 For the OXPHOS inhibition assay, RAW264.7 macrophage cells were treated with UK5099 (10
532 μM, Sigma-Aldrich, dissolved in DMSO 3 h prior to 1st or 2nd rounds of 2-AA exposure.
533 RAW264.7 macrophages supplemented with ATP (20 μM, Sigma-Aldrich, dissolved in PBS)
534 received ATP at the time of 1st and 2nd 2-AA exposure.

535 **Co-Immunoprecipitation assay**

536 For all immunoprecipitation assays, protein A/G agarose Magnetic beads (Pierce) were used
537 after washing in 1X IP buffer. Nuclear lysates from RAW 264.7 tolerized cells exposed to 2-AA
538 for 24 h or non-exposed cells were diluted in 1X IP buffer and 500 μg of protein was taken for
539 each experiment. The lysates were precleared by using unbound 50 μl protein A/G magnetic
540 beads for 2 h at room temperature on a rotator. Precleared lysates were either incubated with
541 ERRα, PGC-1α or rabbit IgG antibody overnight at 4 °C. 100 μl protein A/G magnetic beads
542 were used to pull down the antibody-protein complex and washed twice with IP buffer to
543 remove unbound proteins. Magnetic beads were then eluted in 2X Laemmli SDS-PAGE
544 loading buffer. Immunoprecipitated ERRα and PGC-1α was detected by Western blot
545 analyses, using conformational specific Anti Rabbit antibody (TruBlot).

546 **Immunoblotting analysis**

547 Cells were plated at 6×10^5 cells per well in six-well plates. Cells were washed with PBS and
548 subsequently lysed using RIPA lysis buffer containing 1 mM phenylmethylsulfonyl fluoride
549 (PMSF). 20μg of proteins were separated by electrophoresis on any KD (Kilo Dalton) (Bio-
550 Rad, Cat no. 4569033) SDS-polyacrylamide gel. Proteins were transferred to a 0.2 μm
551 polyvinylidene fluoride membrane (PVDF, Millipore, Billerica, USA) using a Bio-Rad semi-dry
552 instrument. After blocking with 5% BSA in TBS containing 0.1% Tween-20 for 1 h at room
553 temperature, the membranes were incubated with a primary antibody ERR-a (Abcam,
554 #ab76228), MPC1 (D2L91, Cell signaling), and anti-β-actin (cat no: sc-47778) (Santa Cruz
555 Biotechnology) overnight at 4°C. Following washing, the membranes were incubated with an

556 anti-rabbit secondary antibody, and the bands were detected by SuperSignal West Pico
557 Chemiluminescent Substrate (Thermo Scientific) reaction, according to the manufacturer's
558 instructions. The blots were visualized in the ChemiDOC Imaging system (Bio-Rad
559 Laboratories, Inc., Hercules, CA, USA). The bands were analyzed densitometrically using
560 QuantityOne software (Bio-Rad).

561 **Chromatin immunoprecipitation (ChIP) and ChIP-qPCR**

562 For ChIP studies, RAW264.7 macrophage cells exposed to 2-AA for 24 h were cross-linked in
563 1% (v/v) methanol-free formaldehyde for 10 min and then placed in 0.125 M glycine for 5 min
564 at RT. Using the truChIP High Cell Chromatin Shearing kit (Covaris, United States), cells were
565 prepared for sonication according to the Covaris protocol. Approximately 1×10^7 cells were
566 plated in a 12 mm × 12 mm tube and subjected to shearing with the Covaris S220 sonicator for
567 8 min (140 peak power, 5 duty factor, 200 cycles/burst). The Magna ChIP A/G kit (Millipore,
568 United States) was used for the subsequent immunoprecipitations according to the
569 manufacturer's protocol. Briefly, chromatin from approximately 10^6 cells was incubated
570 overnight at 4°C with 2 μg of anti-ERRα or anti-PGC-1α (Abcam, USA) ChIP-grade antibody
571 and 20 μL of A/G magnetic beads. The beads were washed serially (5 min each) with low-salt
572 wash buffer, high-salt wash buffer, LiCl wash buffer, and TE buffer from the kit at 4°C.
573 Chromatin was eluted with elution buffer containing Proteinase K at 62°C for 4 h, then
574 incubated at 95°C for 10 min. DNA was isolated by column purification (QIAquick PCR
575 purification kit).

576 Real-time ChIP-qPCR was performed with the Brilliant II SYBR green super mix (Agilent, USA).
577 Forward (AGTGGTGACCTTGAACTTCCC) and reverse (CTGAAGACGACCTTCCCCTT)
578 primers were chosen to amplify a genomic locus of *MPC1* promoter which had a putative ERR
579 binding site (TNAAGGTCA) at 1582 bp upstream of the start site. Normalized values were
580 calculated by the percent-input method relative to the IgG. The assay was performed three
581 times.

582 **RNA extraction and RT-qPCR**

583 Total RNA from all the groups mentioned above was isolated from approximately 2×10^6 cells
584 with the RNeasy minikit (Qiagen, USA), and cDNA was prepared with the iScript Reverse
585 transcription kit (Bio-Rad, USA), as per the manufacturer's instruction. Real-time PCR was
586 conducted using the PowerUP SYBR green Master mix (Applied Biosystem, USA) and primer
587 sets for mouse ERR-α (forward: ACTACGGTGTGGCATCCTGTGA; reverse:
588 GGTGATCTCACACTCATTGGAGG), MPC-1 (forward: CTCCAGAGATTATCAGTGGGCG;
589 reverse: GAGCTACTTCGTTTGTTACATGGC), TNF-α (forward:
590 GGTGCCTATGTCTCAGCCTCTT; reverse: GCCATAGAACTGATGAGAGGGAG) and mouse
591 18S rRNA (forward: GTTCCGACCATAAACGATGCC; reverse:
592 TGGTGGTGCCCTTCCGTCAAT). The transcript levels of all the genes were normalized to
593 18S rRNA with the ΔΔCT method. The relative expression was calculated by normalizing
594 transcript levels to those of PA14 Infected cells. The assay was conducted in triplicate; means
595 and standard deviations were calculated for each group.

596 **Animal infection and metabolites assessment experiments**

597 The full-thickness thermal burn injury and infection (BI) model [17, 18, 70] was used to assess
598 the effect of 2-AA on metabolic alterations in the spleens of six-week-old CD1 male mice and
599 bacterial burden (Charles River Labs, USA). A full-thickness thermal burn injury involving 5-
600 8% of the total body surface area was produced on the shaved mouse abdomen dermis, and
601 an inoculum of ~1×10^4 PA14 and Δ*mvfR* [19] cells in 100 μL of $MgSO_4$ (10 mM) was injected
602 intradermally into the burn eschar. For the groups that received 2-AA, mice were injected
603 intraperitoneally (IP) with 100 μL of 2-AA (6.75 mg/kg). The entire procedure was done under
604 the influence of anesthesia. One of the groups of mice infected with the PA14 isogenic mutant
605 Δ*mvfR* [19] also received 100 μL of 2-AA in PBS (6.75 mg/kg) at the time of infection (Δ*mvfR*
606 +2-AA) and served as an additional control. CFU counts from rectus abdominus muscle
607 (underlying the burn-infected tissue) were assessed in groups of 4 mice each at 1, 5, and 10

608 d post-BI by plating diluted muscle homogenate on Pseudomonas isolation agar (Sigma-
609 Aldrich) plates containing rifampicin (50 mg/L). Spleen samples from mice were collected for
610 metabolite analyses from all mice groups at 1, 5, and 10 d post-BI to assess ATP (#ab83355
611 Abcam) and acetyl-CoA (#ab87546, Abcam) as described above. Tissues were homogenized,
612 and 100 mg of homogenate was centrifuged at 4°C for 15 min at 10,000 g, and supernatants
613 were collected. The supernatant was mixed with 400 μL of 1 M perchloric acid. The
614 deproteinized supernatant was neutralized by 3 M $KHCO_3$. The ATP and acetyl-CoA assays
615 were performed as described in the *in vitro* section.

616 **Acknowledgments and Funding sources**

617 We thank Dr. Vamsi Mootha and Sneha Rath for access and help with the Seahorse
618 instrument, respectively. This work was supported by the NIH award R01AI134857, The John
619 Lawrence Massachusetts General Hospital Research Scholar Award and Shriner's grant
620 83009 to L.G.R., and the Shriner's grant 85132 to A.A.T. The funders had no role in the study
621 design, data collection, analysis, decision to publish, or manuscript preparation.

622

623 **Figures**

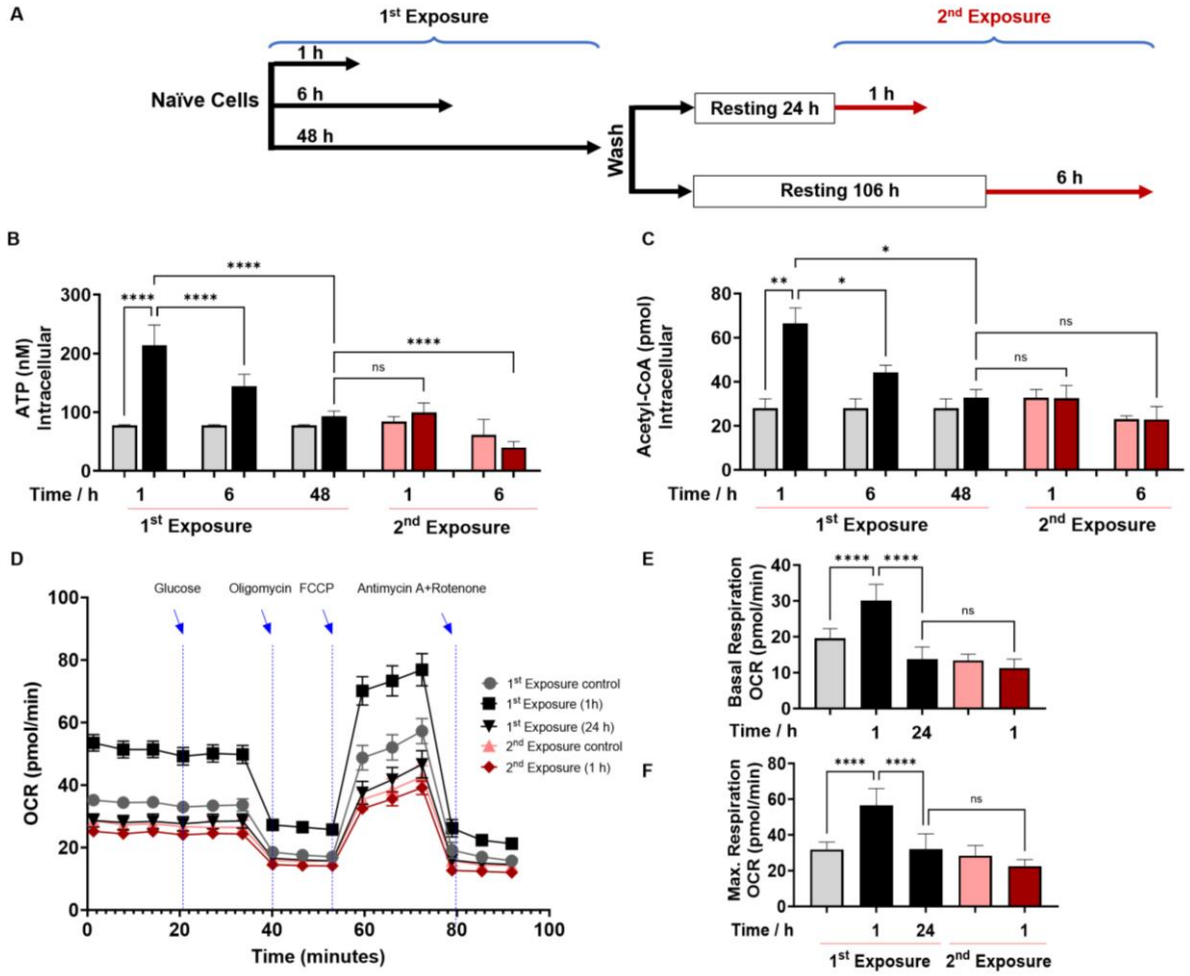

624

625 **Figure 1**

626

627

628

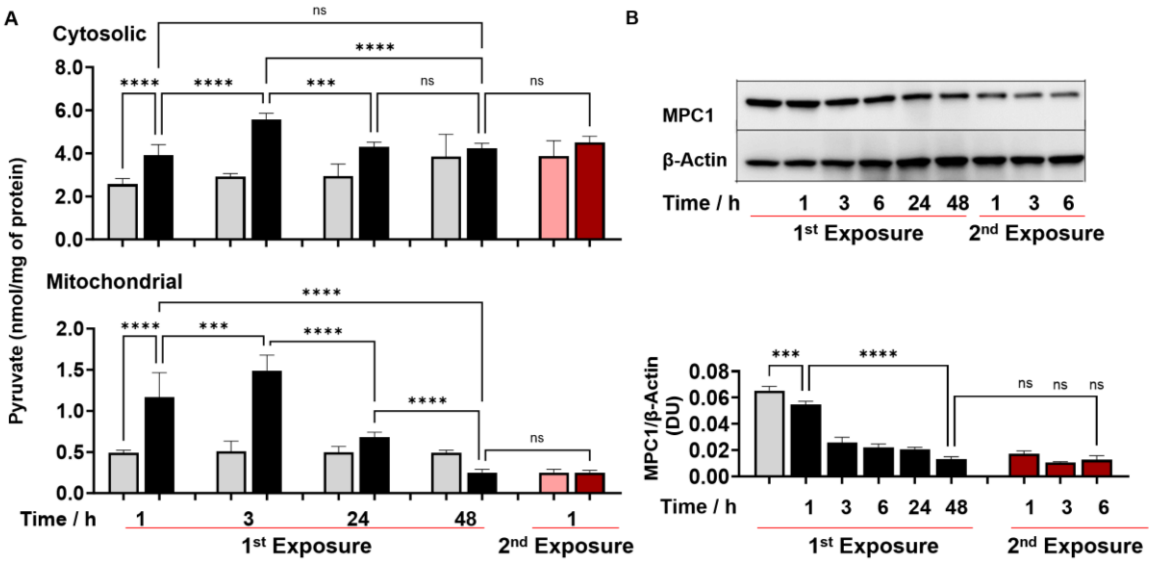

629

630 **Figure 2**

631

632

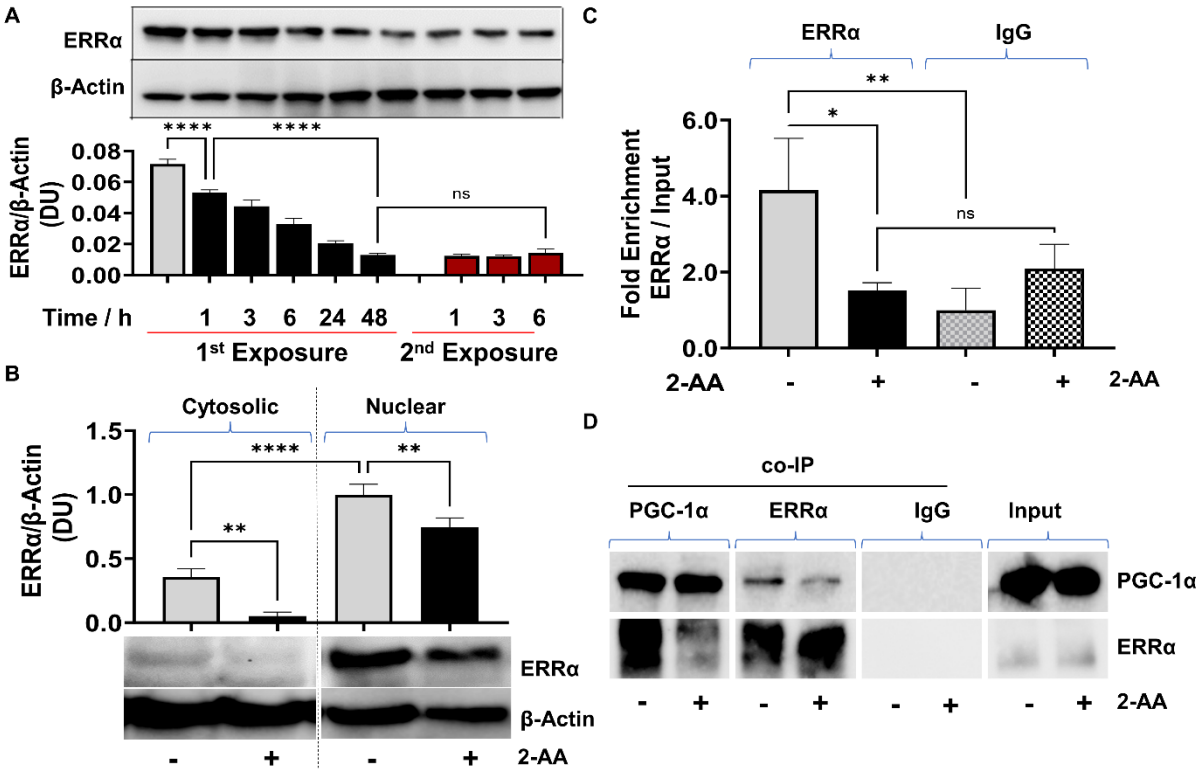

633

634 **Figure 3**

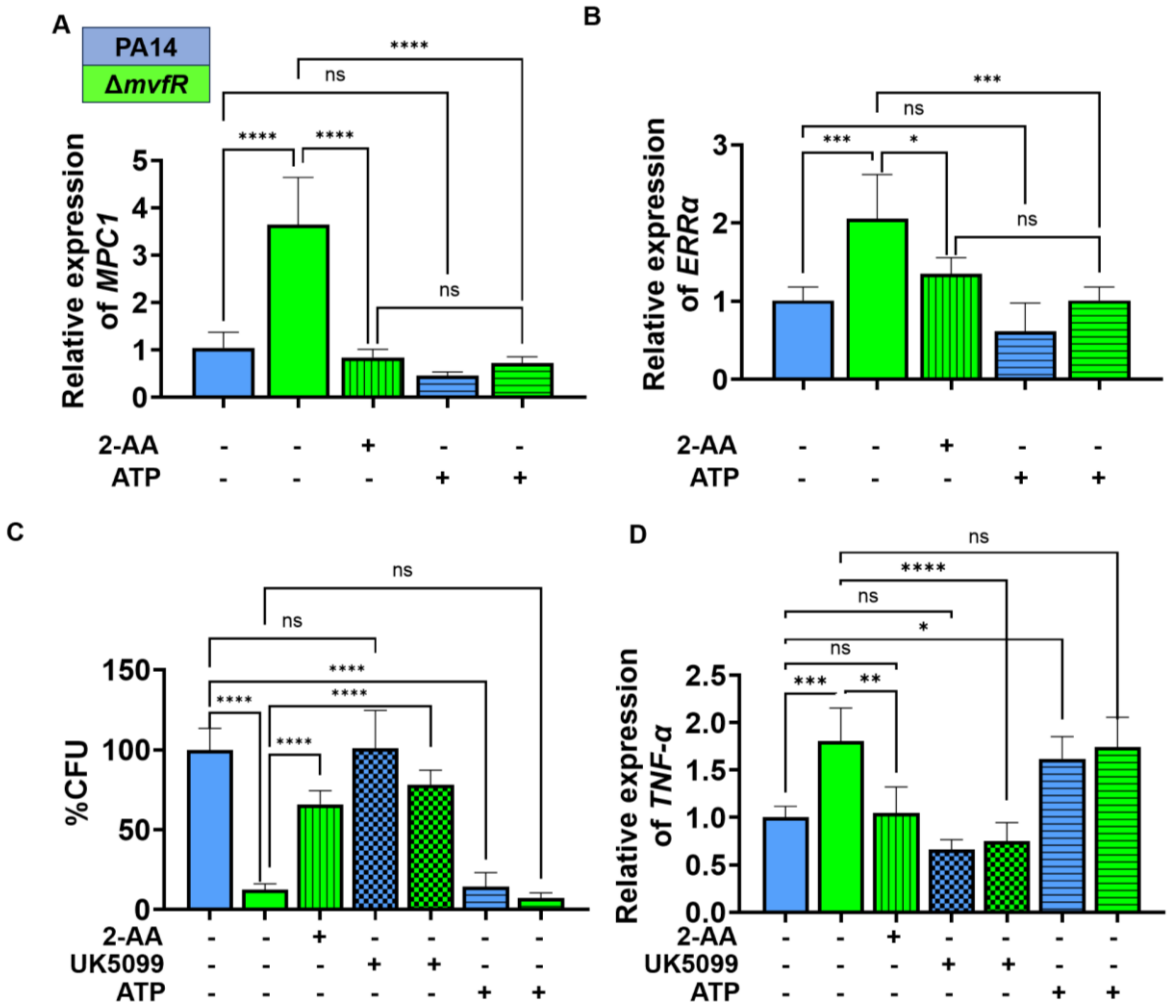

635

636 **Figure 4**

637

638

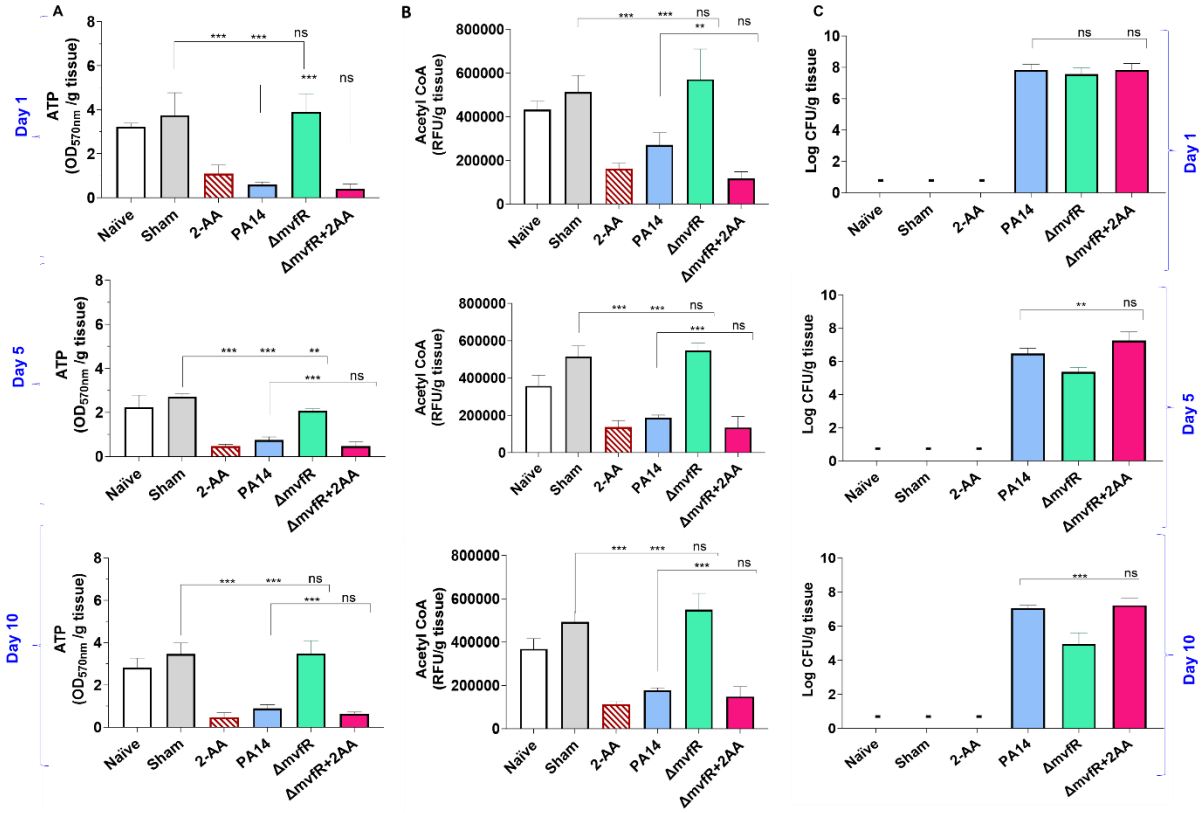

639

640 **Figure 5**

641

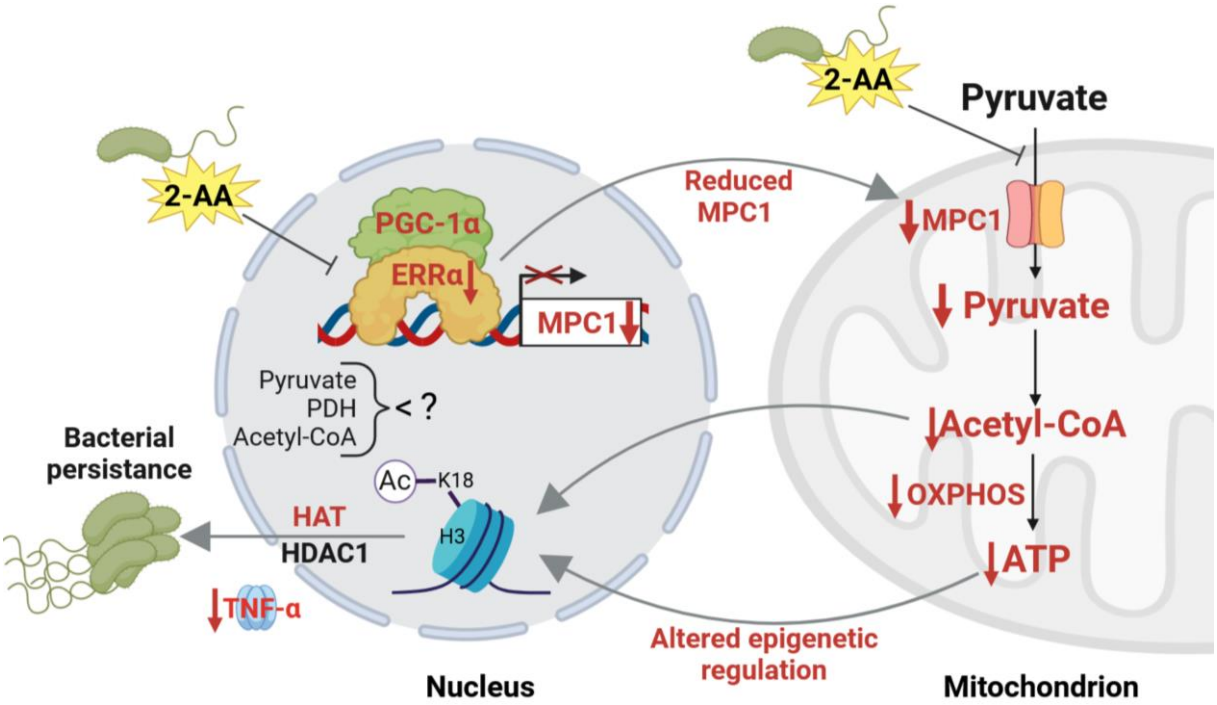
2-AA
2-AA
Pyruvate
Reduced
MPC1
PGC-1α
ERRα
MPC1
MPC1
Pyruvate
Pyruvate
PDH
Acetyl-CoA
< ?
Acetyl-CoA
Bacterial
persistance
Ac
K18
H3
HAT
HDAC1
OXPHOS
ATP
TNF-α
Altered epigenetic
regulation
Nucleus
Mitochondrion

Figure 6

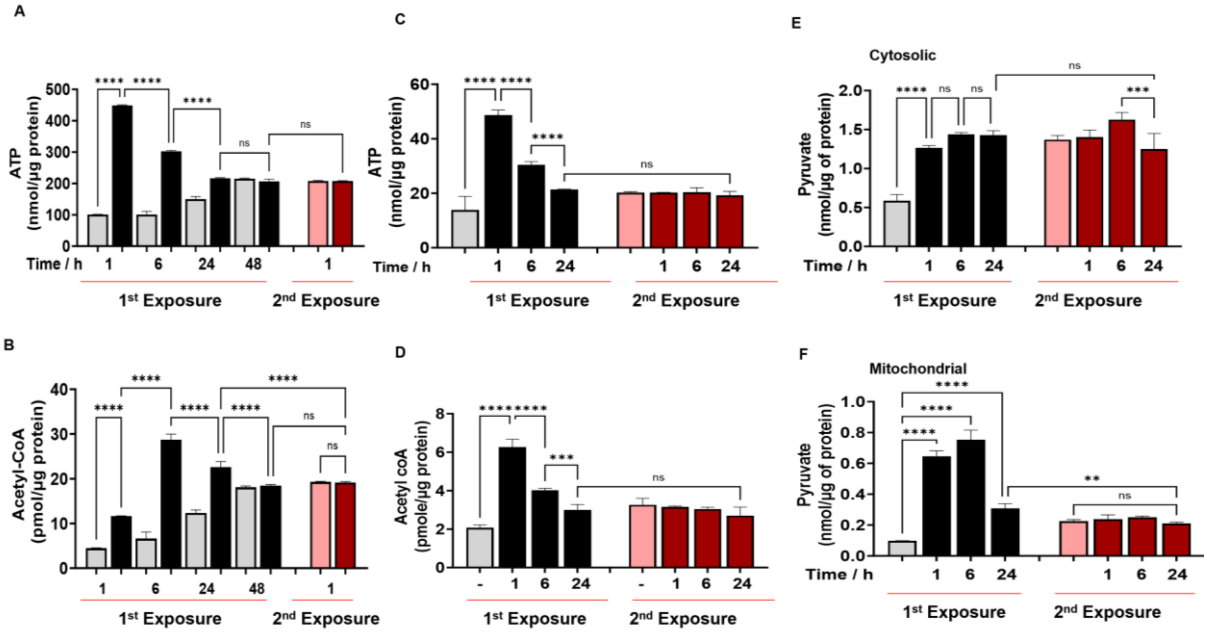

Figure S1

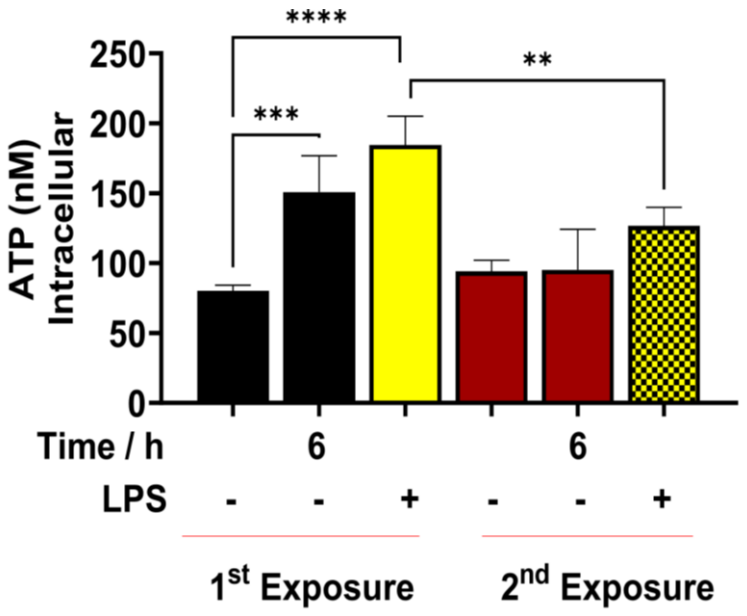

Figure S2

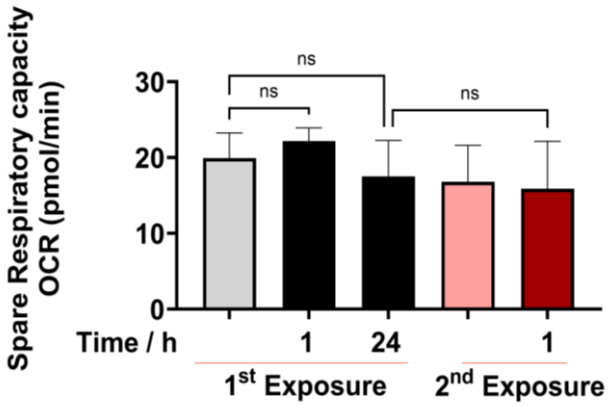
Spare Respiratory capacity
OCR (pmol/min)
30
20
10
0
ns
ns
ns
Time / h
1
24
1
1st Exposure
2nd Exposure

Figure S3

656 **Figure Legends**

657 **Figure 1. 2-AA tolerization decreases crucial metabolites of cellular energy and affects**
658 **mitochondrial respiration in mouse BMDM.** (A) Schematic representation showing
659 experimental design: naïve cells were exposed to 2-AA for 1, 6, or 48 h (black). Cells exposed
660 to 2-AA (400 μM) for 48 h were washed, rested for 24 or 106 h, and re-exposed (200 μM) for
661 1 or 6 h (red), respectively. The same color code: black: cells after 1st exposure; red: cells after
662 2ndexposure, was kept throughout the manuscript with corresponding controls in grey and pink,
663 respectively. The levels of (B) ATP and (C) acetyl-CoA in BMDM cells after 1st and 2nd 2-AA
664 exposure. (D) Real-time oxygen consumption rate (OCR) traces were recorded using a
665 Seahorse XF analyzer and normalized to protein content. Cells were exposed to 2-AA for 1 or
666 24 h (black), washed and rested for 24 h and re-exposed for 1 h (red). Mitochondrial respiratory
667 parameters, (E) basal respiration, and (F) maximal respiration. Data are presented as
668 mean ± SD, n ≥ 4, *p < 0.05, **p < 0.01, ***p < 0.001, and ns indicates no significant difference.
669 One-way ANOVA followed by Tukey's post hoc test was applied.

670 **Figure 2. 2-AA perturbs the mitochondrial MPC1-mediated import and metabolism of**
671 **pyruvate.** (A) Cytosolic and mitochondrial pyruvate levels following 2-AA exposure (black) or
672 re-exposure (red) and corresponding controls in grey and pink respectively, for indicated time
673 points. (B) Representative Western blot and results of densitometric analysis of MPC1 protein
674 levels following 2-AA exposure or re-exposure for indicated time points. β-actin was used as a
675 control. Corresponding controls are shown in grey or pink, respectively. Mean ± SD is shown,
676 n = 3, ***p < 0.001, ****p < 0.0001, and ns indicates no significant difference. One-way ANOVA
677 followed by Tukey's post hoc test was applied.

678 **Figure 3: 2-AA-mediated macrophage tolerization deranges PGC-1α/ERRα-dependent**
679 **metabolic programing.** (A) Representative Western blot and results of densitometric analysis
680 of ERRα protein levels following 2-AA exposure or re-exposure for indicated time points. β-

681 actin was used as a control. (B) Western blots and its corresponding densitometric analysis of
682 ERRα in cytoplasmic or nuclear lysates of tolerized macrophages exposed to 2-AA for 24 h or
683 not exposed to 2-AA. (C) ChIP-qPCR assay of ERRα binding at the MPC1 promoter in RAW
684 264.7 tolerized macrophages exposed to 2-AA (200 μM) for 24 h (black) compared to untreated
685 control macrophages (grey). IgG served as a negative control (D) Representative Western blot
686 of co-immunoprecipitation (co-IP) studies of ERRα and PGC-1α in nuclear extracts of 2-AA
687 tolerized (24 h) and control RAW 264.7 cells. Pull down with IgG served as a negative control.
688 2-AA tolerized macrophages are shown in black, and untreated control macrophages in grey.
689 Mean ± SD in shown, n ≥ 3, *$p < 0.05$, **$p < 0.01$, ****$p < 0.0001$, and ns indicates no significant
690 difference. One-way ANOVA followed by Tukey's post hoc test was applied.

691 **Figure 4: Increased intracellular burden in macrophages is associated with decreased**
692 **expression of *MPC1, ERR-α,* and *TNF-α genes*.** Real-time PCR analysis of *MPC1* (A) and
693 *ERR-α* (B) expression in RAW 246.7 macrophages infected with PA14 or *ΔmvfR* in the
694 presence or absence of exogenous addition of 2-AA or ATP for 6 h as indicated. Transcript
695 levels were normalized to 18srRNA. PA14 infected cells served as controls. (C) Intracellular
696 burden of PA14 or Δ*mvfR* of infected macrophages in the presence or absence of exogenous
697 addition of 2-AA, UK5099, or ATP. Untreated cells infected with PA14 were set as 100%. D)
698 Real-time PCR analysis of TNF-α expression in RAW 246.7 macrophages infected with PA14
699 or Δ*mvfR* in the presence or absence of exogenous addition of 2-AA, ATP, or UK5099.
700 Transcript levels were normalized to 18srRNA. PA14 infected cells served as controls. The
701 compound concentration used for UK5099 was 10 μM and ATP 20 μM. Mean ± SD is shown,
702 $n = 3$, * $p < 0.05$, **$p < 0.01$, ***$p < 0.001$, ****$p < 0.0001$***, and ns indicates no significant
703 difference. One-way ANOVA followed by Tukey's post hoc test was applied.

704 **Figure 5. 2-AA promotes a long-lasting decrease in ATP and acetyl-CoA levels and**
705 **bacterial persistence in *PA*-infected mice.** (A) ATP and (B) acetyl-CoA concentrations in the

706 spleens of mice infected with *PA* wild type (PA14), the isogenic mutant Δ*mvfR*, Δ*mvfR* injected
707 with 2-AA at the time of infection (Δ*mvfR* + 2-AA), or non-infected but injected with 2-AA (6.75
708 mg/kg). (C) Bacterial burden in muscles expressed as CFU count was analyzed using the
709 Kruskal–Wallis non-parametric test with Dunn's post-test; ***$p < 0.001$, and ns indicates no
710 significant difference. Control mice groups: naïve were not given 2-AA; mice receiving 2-AA
711 were given a single intraperitoneal injection of 2-AA; sham represents a burn/PBS group since
712 the burn and infection model was used. Results of three independent replicates with 4 mice
713 per group for 1, 5, and 10 d are shown. Means ± SD are shown, *$p < 0.05$, **$p < 0.01$, ***$p <$
714 0.001, and ns indicate no significant difference. One-way ANOVA followed by Tukey's post hoc
715 test was applied.

716

717 **Figure 6: Proposed mechanism by which 2-AA impairs bioenergetics through the**
718 **inhibition of MPC1-mediated pyruvate transport into mitochondria and its impact on the**
719 **PGC-1α/ERRα axis.** 2-AA tolerized macrophages exhibit diminished pyruvate levels in
720 mitochondria due to the decreased expression of *MPC1*, a consequence of the 2-AA impact
721 on the interaction of ERRα with the transcriptional coactivator PGC-1α for the effective
722 transcription of ERRα, since ERRα controls its own transcription and that of MPC1. In the
723 presence of 2-AA, the weakened interaction between ERRα and PGC-1α results in reduced
724 expression of MPC1 and ERRα. The reduction in mitochondrial pyruvate levels leads to
725 decreased acetyl-CoA and ATP levels, which modulate HDAC1- and HAT-catalyzed
726 remodeling of H3K18 acetylation. The diminished levels of this epigenetic mark have
727 previously been associated with an increased intracellular presence of bacteria in
728 macrophages, as demonstrated by our group [18]. Pathways, proteins, and metabolites that
729 are negatively affected are indicated in red, while positively affected are denoted in black. The
730 figure was created using BioRender.com.

731 **Figure S1.** 2-AA tolerization decreases metabolites in murine RAW 264.7 (A-B) and human
732 THP-1 (C-D) cells. (A and C) ATP, (B and D) acetyl-CoA and (E) cytosolic and (F) mitochondrial
733 pyruvate levels were quantified in 2-AA (400 μM) exposed and re-exposed cells for the hours
734 indicated using the same condition as shown in Fig. 1A. Mean ± SD is shown (n = 3); *** p <
735 0.001, and ns indicates no significant difference. One-way ANOVA followed by Tukey's post
736 hoc test was applied. The same color code: black, cells after 1st exposure; red, cells after 2nd
737 exposure was kept as throughout the main manuscript with corresponding controls shown in
738 grey and pink, respectively.

739 **Figure S2:** ATP levels in murine BMDM (A) cells with and without 2-AA (400 μM) or LPS
740 stimulation (100 μg/mL). Each dot represents 1 experimental replicate of 4 independent
741 experiments (n = 4). Data are presented as mean ± SD, **p < 0.01, ***p < 0.001, and ns
742 indicates no significant difference. One-way ANOVA followed by Tukey's post hoc test was
743 applied.

744 **Figure S3**: Effect of 2-AA on mitochondrial spare respiratory capacity in BMDM non-tolerized
745 (black) and tolerized (red) macrophages. Controls are shown in grey and pink, respectively.
746 Mitochondrial spare respiratory capacity data extrapolated from the OCR profiles shown in
747 Figure 1D. Unstimulated BMDM macrophages were used as a control (c). Means ± SDs are
748 shown, n = 6, * p < 0.05, *** p < 0.001, and ns indicates no significant difference. One-way
749 ANOVA followed by Tukey's post hoc test was applied.

750

751

752

753 **References**

754 1. Foster, S.L., D.C. Hargreaves, and R. Medzhitov, *Gene-specific control of inflammation by tlr-*
755 *induced chromatin modifications.* Nature, 2007. **447**(7147): p. 972.
756 2. Bagchi, A., et al., *Myd88-dependent and myd88-independent pathways in synergy, priming,*
757 *and tolerance between tlr agonists.* Journal of immunology, 2007. **178**(2): p. 1164.
758 3. Masyutina, A.M., et al., *Inhibition of specific signaling pathways rather than epigenetic*
759 *silencing of effector genes is the leading mechanism of innate tolerance.* Frontiers in
760 Immunology, 2023. **14**.
761 4. O'Neill, L.A., R.J. Kishton, and J. Rathmell, *A guide to immunometabolism for immunologists.*
762 Nat Rev Immunol, 2016. **16**(9): p. 553.
763 5. Chi, H., *Immunometabolism at the intersection of metabolic signaling, cell fate, and systems*
764 *immunology.* Cell Mol Immunol, 2022. **19**(3): p. 299.
765 6. Tannahill, G.M., et al., *Succinate is an inflammatory signal that induces il-1beta through hif-*
766 *1alpha.* Nature, 2013. **496**(7444): p. 238.
767 7. Galli, G. and M. Saleh, *Immunometabolism of macrophages in bacterial infections.* Front Cell
768 Infect Microbiol, 2020. **10**: p. 607650.
769 8. Wang, Y., et al., *Mitochondrial metabolism regulates macrophage biology.* J Biol Chem, 2021.
770 **297**(1): p. 100904.
771 9. Karan, K.R., et al., *Leukocyte cytokine responses in adult patients with mitochondrial DNA*
772 *defects.* Journal of Molecular Medicine, 2022. **100**(6): p. 963.
773 10. Bird, L., *Getting enough energy for immunity.* Nat Rev Immunol, 2019. **19**(5): p. 269.
774 11. Deziel, E., et al., *The contribution of mvfr to pseudomonas aeruginosa pathogenesis and*
775 *quorum sensing circuitry regulation: Multiple quorum sensing-regulated genes are modulated*
776 *without affecting lasri, rhlri or the production of n-acyl-l-homoserine lactones.* Mol Microbiol,
777 2005. **55**(4): p. 998.
778 12. Xiao, G., et al., *Mvfr, a key pseudomonas aeruginosa pathogenicity lttr-class regulatory*
779 *protein, has dual ligands.* Mol Microbiol, 2006. **62**(6): p. 1689.
780 13. Eickhoff, M.J. and B.L. Bassler, *Snapshot: Bacterial quorum sensing.* Cell, 2018. **174**(5): p.
781 1328.
782 14. Fuqua, C. and E.P. Greenberg, *Listening in on bacteria: Acyl-homoserine lactone signalling.*
783 Nature Reviews Molecular Cell Biology, 2002. **3**(9): p. 685.
784 15. Kariminik, A., M. Baseri-Salehi, and B. Kheirkhah, *Pseudomonas aeruginosa quorum sensing*
785 *modulates immune responses: An updated review article.* Immunol Lett, 2017. **190**: p. 1.
786 16. Liu, Y.C., K.G. Chan, and C.Y. Chang, *Modulation of host biology by pseudomonas aeruginosa*
787 *quorum sensing signal molecules: Messengers or traitors.* Front Microbiol, 2015. **6**: p. 1226.
788 17. Bandyopadhaya, A., et al., *The quorum sensing volatile molecule 2-amino acetophenon*
789 *modulates host immune responses in a manner that promotes life with unwanted guests.*
790 PLoS pathogens, 2012. **8**(11): p. e1003024.
791 18. Bandyopadhaya, A., et al., *A quorum-sensing signal promotes host tolerance training through*
792 *hdac1-mediated epigenetic reprogramming.* Nat Microbiol, 2016. **1**: p. 16174.
793 19. Cao, H., et al., *A quorum sensing-associated virulence gene of pseudomonas aeruginosa*
794 *encodes a lysr-like transcription regulator with a unique self-regulatory mechanism.* Proc Natl
795 Acad Sci U S A, 2001. **98**(25): p. 14613.
796 20. Deziel, E., et al., *Analysis of pseudomonas aeruginosa 4-hydroxy-2-alkylquinolines (haqs)*
797 *reveals a role for 4-hydroxy-2-heptylquinoline in cell-to-cell communication.* Proc Natl Acad Sci
798 U S A, 2004. **101**(5): p. 1339.
799 21. Kesarwani, M., et al., *A quorum sensing regulated small volatile molecule reduces acute*
800 *virulence and promotes chronic infection phenotypes.* PLoS pathogens, 2011. **7**(8): p.
801 e1002192.

22. Bandyopadhaya, A., A. Tsurumi, and L.G. Rahme, *Nf-kappabp50 and hdac1 interaction is implicated in the host tolerance to infection mediated by the bacterial quorum sensing signal 2-aminoacetophenone.* Front Microbiol, 2017. **8**: p. 1211.
23. Wheeler, D.S., et al., *Induction of endotoxin tolerance enhances bacterial clearance and survival in murine polymicrobial sepsis.* Shock, 2008. **30**(3): p. 267.
24. Tzika, A.A., et al., *A small volatile bacterial molecule triggers mitochondrial dysfunction in murine skeletal muscle.* PloS one, 2013. **8**(9): p. e74528.
25. Bandyopadhaya, A., et al., *Bacterial-excreted small volatile molecule 2-aminoacetophenone induces oxidative stress and apoptosis in murine skeletal muscle.* International Journal of Molecular Medicine, 2016. **37**(4): p. 867.
26. Chakraborty, A., et al., *Quorum-sensing signaling molecule 2-aminoacetophenone mediates the persistence of pseudomonas aeruginosa in macrophages by interference with autophagy through epigenetic regulation of lipid biosynthesis.* mBIo, 2023: p. e0015923.
27. Maurice, N.M., et al., *Pseudomonas aeruginosa induced host epithelial cell mitochondrial dysfunction.* Scientific Reports, 2019. **9**(1).
28. Lelliott, C.J. and A. Vidal-Puig, *Pgc-1beta: A co-activator that sets the tone for both basal and stress-stimulated mitochondrial activity.* Adv Exp Med Biol, 2009. **646**: p. 133.
29. Supruniuk, E., A. Mikłosz, and A. Chabowski, *The implication of pgc-1α on fatty acid transport across plasma and mitochondrial membranes in the insulin sensitive tissues.* Front Physiol, 2017. **8**: p. 923.
30. Coppi, L., et al., *Pgc1s and beyond: Disentangling the complex regulation of mitochondrial and cellular metabolism.* Int J Mol Sci, 2021. **22**(13): p. 6913.
31. Lin, J., C. Handschin, and B.M. Spiegelman, *Metabolic control through the pgc-1 family of transcription coactivators.* Cell Metab, 2005. **1**(6): p. 361.
32. Huss, J.M., W.G. Garbacz, and W. Xie, *Constitutive activities of estrogen-related receptors: Transcriptional regulation of metabolism by the err pathways in health and disease.* Biochim Biophys Acta, 2015. **1852**(9): p. 1912.
33. Schreiber, S.N., et al., *The transcriptional coactivator pgc-1 regulates the expression and activity of the orphan nuclear receptor estrogen-related receptor alpha (erralpha).* J Biol Chem, 2003. **278**(11): p. 9013.
34. Laganiere, J., et al., *A polymorphic autoregulatory hormone response element in the human estrogen-related receptor alpha (erralpha) promoter dictates peroxisome proliferator-activated receptor gamma coactivator-1alpha control of erralpha expression.* J Biol Chem, 2004. **279**(18): p. 18504.
35. Villena, J.A., *New insights into pgc-1 coactivators: Redefining their role in the regulation of mitochondrial function and beyond.* FEBS J, 2015. **282**(4): p. 647.
36. Ranhotra, H.S., *The estrogen-related receptor alpha: The oldest, yet an energetic orphan with robust biological functions.* J Recept Signal Transduct Res, 2010. **30**(4): p. 193.
37. Deblois, G. and V. Giguere, *Functional and physiological genomics of estrogen-related receptors (errs) in health and disease.* Biochim Biophys Acta, 2011. **1812**(8): p. 1032.
38. Ranhotra, H.S., *The estrogen-related receptors: Orphans orchestrating myriad functions.* J Recept Signal Transduct Res, 2012. **32**(2): p. 47.
39. Charest-Marcotte, A., et al., *The homeobox protein prox1 is a negative modulator of erralpha/pgc-1alpha bioenergetic functions.* Genes Dev, 2010. **24**(6): p. 537.
40. Eichner, L.J. and V. Giguere, *Estrogen related receptors (errs): A new dawn in transcriptional control of mitochondrial gene networks.* Mitochondrion, 2011. **11**(4): p. 544.
41. Koh, E., et al., *Mpc1 is essential for pgc-1alpha-induced mitochondrial respiration and biogenesis.* Biochem J, 2018. **475**(10): p. 1687.
42. Divangahi, M., et al., *Trained immunity, tolerance, priming and differentiation: Distinct immunological processes.* Nat Immunol, 2021. **22**(1): p. 2.

43. Koh, E., et al., *Mpc1 is essential for pgc-1α-induced mitochondrial respiration and biogenesis.* Biochem J, 2018. **475**(10): p. 1687.
44. Xue, C., et al., *Mitochondrial pyruvate carrier 1: A novel prognostic biomarker that predicts favourable patient survival in cancer.* Cancer Cell Int, 2021. **21**(1): p. 288.
45. Bronte, V. and M.J. Pittet, *The spleen in local and systemic regulation of immunity.* Immunity, 2013. **39**(5): p. 806.
46. Starkey, M., et al., *Identification of anti-virulence compounds that disrupt quorum-sensing regulated acute and persistent pathogenicity.* PLoS pathogens, 2014. **10**(8): p. e1004321.
47. Dulcey, C.E., et al., *The end of an old hypothesis: The pseudomonas signaling molecules 4-hydroxy-2-alkylquinolines derive from fatty acids, not 3-ketofatty acids.* Chem Biol, 2013. **20**(12): p. 1481.
48. Fetzner, S. and S.L. Drees, *Old molecules, new biochemistry.* Chem Biol, 2013. **20**(12): p. 1438.
49. Park, S., et al., *Inhibition of erralpha prevents mitochondrial pyruvate uptake exposing nadph-generating pathways as targetable vulnerabilities in breast cancer.* Cell Rep, 2019. **27**(12): p. 3587.
50. Caslin, H.L., et al., *Lactate is a metabolic mediator that shapes immune cell fate and function.* Front Physiol, 2021. **12**: p. 688485.
51. Lee, T.Y., *Lactate: A multifunctional signaling molecule.* Yeungnam Univ J Med, 2021. **38**(3): p. 183.
52. Li, X., et al., *Lactate metabolism in human health and disease.* Signal Transduct Target Ther, 2022. **7**(1): p. 305.
53. Wei, W., et al., *Ligand activation of erralpha by cholesterol mediates statin and bisphosphonate effects.* Cell Metab, 2016. **23**(3): p. 479.
54. Chisamore, M.J., et al., *Identification of small molecule estrogen -related receptor α–specific antagonists and homology modeling to predict the molecular determinants as the basis for selectivity over errβ and errγ.* Drug development research, 2008. **69**(4): p. 203.
55. Kushwaha, A., V. Kumar, and V. Agarwal, *Pseudomonas quinolone signal induces organelle stress and dysregulates inflammation in human macrophages.* Biochim Biophys Acta Gen Subj, 2023. **1867**(2): p. 130269.
56. Pietrocola, F., et al., *Acetyl coenzyme a: A central metabolite and second messenger.* Cell Metab, 2015. **21**(6): p. 805.
57. Chandran, A., et al., *Mycobacterium tuberculosis infection induces hdac1-mediated suppression of il-12b gene expression in macrophages.* Front Cell Infect Microbiol, 2015. **5**: p. 90.
58. Shi, L. and B.P. Tu, *Acetyl-coa and the regulation of metabolism: Mechanisms and consequences.* Curr Opin Cell Biol, 2015. **33**: p. 125.
59. Lauterbach, M.A., et al., *Toll-like receptor signaling rewires macrophage metabolism and promotes histone acetylation via atp-citrate lyase.* Immunity, 2019. **51**(6): p. 997.
60. Saeed, S., et al., *Epigenetic programming of monocyte-to-macrophage differentiation and trained innate immunity.* Science, 2014. **345**(6204): p. 1251086.
61. Liu, T.F., et al., *Nad+-dependent sirtuin 1 and 6 proteins coordinate a switch from glucose to fatty acid oxidation during the acute inflammatory response.* J Biol Chem, 2012. **287**(31): p. 25758.
62. Ishida, K., et al., *Chlamydia pneumoniae effector chlamydial outer protein n sequesters fructose bisphosphate aldolase a, providing a benefit to bacterial growth.* BMC Microbiol, 2014. **14**: p. 330.
63. Kunze, M., et al., *Metabolic adaption of legionella pneumophila during intracellular growth in acanthamoeba castellanii.* Int J Med Microbiol, 2021. **311**(4): p. 151504.
64. Shi, L., et al., *Infection with mycobacterium tuberculosis induces the warburg effect in mouse lungs.* Sci Rep, 2015. **5**: p. 18176.

65. Perez-Morales, D. and V.H. Bustamante, *Cross-kingdom metabolic manipulation promotes salmonella replication inside macrophages.* Nat Commun, 2021. **12**(1): p. 1862.
66. Dhamgaye, S., Y. Qu, and A.Y. Peleg, *Polymicrobial infections involving clinically relevant gram-negative bacteria and fungi.* Cell Microbiol, 2016. **18**(12): p. 1716.
67. Vega, R.B., J.M. Huss, and D.P. Kelly, *The coactivator pgc-1 cooperates with peroxisome proliferator-activated receptor alpha in transcriptional control of nuclear genes encoding mitochondrial fatty acid oxidation enzymes.* Molecular and cellular biology, 2000. **20**(5): p. 1868.
68. Van den Bossche, J., J. Baardman, and M.P. de Winther, *Metabolic characterization of polarized m1 and m2 bone marrow-derived macrophages using real-time extracellular flux analysis.* J Vis Exp, 2015(105): p. e53424.
69. Rahme, L.G., et al., *Common virulence factors for bacterial pathogenicity in plants and animals.* Science, 1995. **268**(5219): p. 1899.
70. Maura, D., A. Bandyopadhaya, and L.G. Rahme, *Animal models for pseudomonas aeruginosa quorum sensing studies.* Methods Mol Biol, 2018. **1673**: p. 227.